JOURNAL OF AIRCRAFT
Vol. 32, No. 4, July–August 1995

Numerical Analysis of the Vortical Flow Around a Delta Wing-Canard Configuration

A. Das* and J. M. A. Longo†
DLR, German Aerospace Research Establishment, Braunschweig D-38022, Germany

In this article a numerical study of the vortical flows around a delta-shaped wing, with and without canard, is undertaken by solving the Euler equations. The analysis elucidates the essential physics that are involved in establishing the complex vortical flows around the configurations, especially with the required radial pressure gradients that provide the accelerating forces for spiraling. Further emphasis is put in studying the flow gradients arising over the wing surface and along the vortex axis. An interesting physical feature is the occurrence of two saddle points on the vortex axis at high angles of incidence, one causing flow reversal and the other the vortex bursting. The beneficial effect of the canard vortex on the wing vortex has been clearly demonstrated, it leads to a significant retardation of the vortex bursting. All essential experimental findings known until now have been closely reproduced, and thus, confirmed and elucidated by the numerical results.

Nomenclature

A = Jacobian matrix
a, a^* = local and critical speed of sound
b = span of a wing
c_L, c_D, c_M = total lift, drag, and moment coefficient
c_p = pressure coefficient
$\bar{c}_p, \bar{c}_V$ = specific heats
D = dissipation operator
E = energy content in unit mass of the medium
e = internal heat energy in unit mass of the medium
F, G, H = flux quantities in x, y, and z directions
$\bar{F}, \bar{G}, \bar{H}$ = flux quantities in ξ, η, and ζ directions
f_a = accelerating force per unit mass in a spiraling flow
h, h_0 = static and total enthalpy in unit mass of the medium
i, j, k = grid notations
J = determinant of Jacobian matrix
k = heat flow coefficient
$l(\eta), l_0$ = chord length and total length of a delta wing
M, M_∞ = local and onflow Mach number
M^* = Mach number based on critical speed of sound
$\boldsymbol{n}$ = normal to a surface
p, p_∞ = static pressure in the spiraling flow and in the onflow
$p_0, p_{0,\infty}$ = total pressure in the spiraling flow and in the onflow
Q = flux balance in elemental volume
$\bar{q}$ = heat flow
R = gas constant
r, r_0 = radial distance in the spiraling vortex and to the wing leading edge
S = surface area
S_w, S_c = surface area of the wing and canard
s = entropy
$\bar{s}(\xi), \bar{s}$ = local and maximum half-span of the wing
T, T_0 = static and total temperature in the flowfield
t = time
U = physical variables in a flowfield
u, v, w = velocity components in Cartesian coordinates
V, V_∞ = local and onflow velocity
v_a = axial velocity along the vortex core
v_c, v_h = crossflow and helical velocity in the spiraling vortex
v_r, v_ϑ, v_x = velocity components in cylindrical coordinates
X^i = physical coordinates
x, r, ϑ = cylindrical coordinates
x, y, z = Cartesian coordinates
α = angle of incidence
β = angle of yaw
γ = vorticity in the flowfield
ε = geometric setting angle of the canard
κ = ratio of specific heats
$\bar{\nu}$ = pressure sensor in the dissipative operator
ξ, η, ζ = curvilinear coordinates
ρ, ρ_0 = static and stagnation medium density
$\boldsymbol{\sigma}_v$ = stress tensor due to viscosity
φ = sweep angle of the wing leading edge
$\boldsymbol{\chi}$ = flux tensor in the flowfield
$\Omega, \tilde{\Omega}$ = volume of a cell element in Cartesian and curvilinear coordinate system

I. Introduction

FOR studying complex flows arising from the motion of bodies in an unbounded medium, it is usual to base these studies on the numerical solutions of Navier–Stokes equations, and more frequently on the Euler equations, when the effects of viscosity and heat conductivity of the medium are small and remain confined to limited regions. For detailed analysis of the physics of the flowfields with systematic parameter variations, it is preferable to use the Euler equations, due to the relatively less computational effort.

The standard numerical procedures that are extensively used now, comprising grid generation, numerical simulation of the partial differential equations and their solution, are considered to be well-established. Some basic numerical methods formulated with finite difference and finite volume schemes as described in Refs. 1–3 are used to solve the Euler equations, while the methods for solving Reynolds-averaged Navier–Stokes equations are dealt with in Refs. 4–6. For turbulent flows it is essential to model the turbulent exchanges producing viscous stresses, for which the classical eddy viscosity concept has proven to be quite useful.

Received June 5, 1994; revision received Dec. 2, 1994; accepted for publication Dec. 8, 1994.

*Advisor, Institut SM-EA and Professor of Fluid Mechanics, Technical University, Braunschweig, Germany. Member AIAA.
†Research Scientist, Institut SM-EA. Member AIAA.

The efficiency of a numerical code is measured by three essential criteria: 1) good accuracy with robustness, 2) acceptable CPU time, and 3) easy applicability to complex flowfields. For good accuracy a primary concern is to ensure a proper numerical simulation of the field equations and of the boundary conditions. For these, a prerequisite is the generation of high-quality field grids around the moving wings and bodies. The efficiency of the grid generation technique is measured by the smoothness and orthogonality of the meshes and required grid fineness, especially in regions of high flow gradients. Some basic methods that are now widely in use to produce acceptable field grids in body-fitted coordinates follow the procedures described in Refs. 7–9. Successful implementation of the numerical field methods for solving the Euler and Navier–Stokes equations gave a big impetus to study the vortical flows arising over slender delta wings moving with incidence angles, as they bring in a large additional contribution to the lift force, which is termed as vortex lift. Extensive efforts concerning this subject have been made in recent years, as evident from the great number of published papers.[10–19]

The vortical flowfields of the delta wings are characterized by two basic phenomena: 1) the loss of total pressure in the spiraling flows as a function incidence angle and Mach number and 2) the breakdown of the vortical structure of the flow at high incidence angles, the latter causing a loss in the additional vortex-lift. These phenomena are little affected by the viscosity of the medium, as has been confirmed by the numerical solutions of the Euler and Navier–Stokes equations as well as by the experimental results. Some useful insights into the physics of these interesting phenomena are given.[14]

Further subjects of numerical studies have been the flowfields of double-delta or strake wings,[20,21] while extensive studies on the flowfields of delta-shaped wing-canard combinations are made in Refs. 22–27. The experimental works that are useful to validate the results of numerical studies are cited in Refs. 28–36, these being, however, mostly confined to specific and limited speed ranges at each test.

For the physics of inviscid and viscous flowfields with vortex formation, classical literature[37–41] contain some basic foundations, whereas for the numerical treatment of the partial differential equations, Ref. 42 proves to be quite useful.

The subject of this article is to undertake a detailed numerical analysis on the physics of the vortical flowfields, especially for a delta-shaped wing-canard configuration. Besides reproducing the experimental findings, the analysis explains the physical conditions that are needed to establish the spiraling flows, and elucidate the nature of vortex interactions, which leads to a suppression of the vortex breakdown to high incidence angles. The findings of these numerical analysis can form the basis for achieving an efficient wing-canard configuration with outstanding aerodynamic properties.

II. Basic Equations Describing the Flowfields of Bodies Moving in an Unbounded Medium

The disturbance fields arising from motions of bodies in a compressible viscous medium are essentially described by the Navier–Stokes equations, based on the conservation laws of mass, momentum, and energy in an elementary volume moving with the coordinate system. The field equations can be written in divergence form with the dependable variables ρ, ρu, ρv, ρw, and ρE, or alternately in nondivergence form. In the latter case the equations can also be reduced in terms of the primary variables ρ, u, v, w, and p. For the numerical solution of these equations it is purposeful to use body-fitted curvilinear coordinates for having desirable field grids and better fulfillment of the boundary conditions.

A. Flow Equations in Conservation Law Form for Viscous and Nonviscous Medium

For a fluid medium at standard temperature and pressure, the Navier–Stokes equations describing the disturbance field in an unbounded medium can be written in divergence form in the following way:

$$\begin{aligned}
&\frac{\partial \rho}{\partial t} + \operatorname{div}(\rho V) = 0 \\
&\frac{\partial(\rho V)}{\partial t} + \operatorname{div}(V, \rho V) + \operatorname{div}(pI) - \{\operatorname{div} \boldsymbol{\sigma}_v\} = 0 \\
&\frac{\partial(\rho E)}{\partial t} + \operatorname{div}(\rho E V) + \operatorname{div}(pV) - \{\operatorname{div}(k \operatorname{grad} T) \\
&\quad + \operatorname{div}(V \cdot \boldsymbol{\sigma}_v)\} = 0
\end{aligned} \tag{1}$$

with $I = (i:i + j:j + k:k)$ as a unit dyad. The divergence of the momentum flux in the second expression contains a dyadic product comprising all nine components of the flux in the three coordinate directions, with $\boldsymbol{V} = iu + jv + kw$.

Furthermore,

$$E = e + (V^2/2), \qquad p = (\kappa - 1)\rho[E - (V^2/2)] \equiv \rho RT$$

$\boldsymbol{\sigma}_v$ = viscous stress tensor, $\boldsymbol{q} = k \operatorname{grad} T \equiv$ heat flux, and $e = c_v T$.

If the flow is concerned with turbulent exchange of momentum, a major task is to model the viscous stresses $\boldsymbol{\sigma}_v$ in order to have a complete formulation of the mathematical problem. A usual procedure is to use eddy-viscosity modeling.[6] For a perfect medium the terms in the braces drop out, and Eq. (1) reduces to the Euler equations in divergence form.

B. Euler Equations and Their Extended Versions for Detailed Study of Spiraling Vortical Flows

In Eq. (1), if the relation of the first equation is used in the other two, and the terms in braces are neglected, it leads directly to the classical Euler equations known in the literature

$$\begin{aligned}
&\frac{D\rho}{Dt} + \rho \operatorname{div} V = 0 \\
&\rho \frac{DV}{Dt} + \operatorname{grad} p = 0 \\
&\rho \frac{Dh_0}{Dt} - \frac{\partial p}{\partial t} = 0
\end{aligned} \tag{2}$$

where

$$\frac{D}{Dt} = \frac{\partial}{\partial t} + \boldsymbol{V} \cdot \operatorname{grad}$$

For analyzing the accelerating forces in a spiraling flow, it is convenient to have the components of the Euler momentum equations in Eq. (2) expressed in cylindrical coordinates. This can be easily done by using the relations:

$$\operatorname{grad} \equiv i \frac{\partial}{\partial r} + j \frac{1}{r} \frac{\partial}{\partial \vartheta} + k \frac{\partial}{\partial x} \quad \text{and} \quad V = iv_r + jv_\vartheta + kv_x$$

The momentun equation (2) can be rewritten in Lamb's version

$$\frac{DV}{Dt} = \frac{\partial V}{\partial t} + \operatorname{grad} \frac{V^2}{2} + \gamma \times V = -\frac{1}{\rho} \operatorname{grad} p \tag{3}$$

with $\gamma \equiv i\gamma_r + j\gamma_\vartheta + k\gamma_x$.

Adding $c_p \operatorname{grad} T$ to both sides of Eq. (3), the Euler momentum equation can be recast in the Lamb–Crocco version, which reads

$$\frac{\partial V}{\partial t} + \operatorname{grad} h_0 + \gamma \times V = -\frac{1}{\rho} \operatorname{grad} p + c_p \operatorname{grad} T \tag{4}$$

For steady adiabatic flow the second law of thermodynamics yields the following relation for the vorticity in the flowfield:

$$\gamma \times V = c_p \text{ grad } T - (1/\rho)\text{grad } p = T \text{ grad } s \quad (5)$$

Equations (2–5) will be used extensively to analyze the physics of the spiraling flows arising on slender delta wings.

C. Numerical Simulation of the Field Equations and an Outline on the Method of Solution

For the numerical solution of the Euler equations, as expressed in Eq. (1) with the terms in braces being deleted, it is purposeful to write them in a universal vector form:

$$\frac{\partial \boldsymbol{U}}{\partial t} + \nabla \cdot \boldsymbol{\chi} = 0 \quad (6)$$

where the solution vector $\boldsymbol{U}$ and the flux density tensor $\boldsymbol{\chi}$ are defined as

$$\boldsymbol{U} = \begin{bmatrix} \rho \\ \rho u \\ \rho v \\ \rho w \\ \rho E \end{bmatrix} \quad \text{and} \quad \boldsymbol{\chi} = \begin{bmatrix} \rho V \\ \rho u V + p i_x \\ \rho v V + p i_y \\ \rho w V + p i_z \\ \rho E V + p V \end{bmatrix} \quad (7)$$

In Cartesian system of coordinates, the flux tensor has the expression:

$$\boldsymbol{\chi} = F i_x + G i_y + H i_z \quad (8)$$

The Euler equation can be expressed also in integral form by integrating Eq. (6) over an arbitrary volume Ω enclosed by a surface S. If the volume integral of the flux tensor is converted to surface integral by using Gauss theorem, one obtains

$$\frac{\partial \boldsymbol{U}}{\partial t} + \frac{1}{\Omega} \int_S \boldsymbol{\chi} \cdot \boldsymbol{n} \, dS = 0 \quad (9)$$

where $\boldsymbol{U} = 1/\Omega \int \boldsymbol{U} \, d\Omega$, and dS is a surface element of S with $\boldsymbol{n}$ as its unit outer-normal vector. The Euler equations for unsteady flowfields as expressed by Eq. (6) being of hyperbolic type need the specification of the following conditions for the solution of a given problem: 1) the initial condition as prescribed by the onflow at a time $t = t_0$; 2) boundary condition on the solid surface fulfilling the flow tangency condition $V \cdot \boldsymbol{n} = V_\infty \cdot \boldsymbol{n} + v \cdot \boldsymbol{n} = 0$; 3) boundary condition at the far field based on the characteristic relations, so that the propagation of informations from inside and outside are properly matched, thus preventing spurious reflections into the enclosed domain; and 4) the condition of periodicity at the inner cuts used in the solution domain, and also the condition of matching of the flow variables at block boundaries of multiblock grid topologies.

In order to fulfill the boundary conditions at the body surface quite accurately, it is preferable to use body-fitted curvilinear coordinates in the physical space.

For the generation of body-fitted grids, one can refer to the cited literature.[7-9] Depending on the nature of configurations, one has to select the grid topology, which may be of O-O, C-O, H-O, or H-H type. In case of the delta wing configuration, the O-O or C-O grid structures are most preferable, as they yield suitable grid clustering close to the body surface and in the regions of leading and trailing edges in a natural way.

The basic solution scheme for the Euler Eq. (9) follows a finite volume spatial discretization for the flux balance with Runge–Kutta integration in time for the solution vector $\boldsymbol{U}$, as described by Jameson et al.[2] This has been extended and implemented in the DLR–Euler code CEV CATS as a cell vertex discretization,[3] in which $\boldsymbol{U}$ is evaluated at the vertices of the mesh cells. Since the equations are discretized using central differences, this causes a decoupling of the terms for even- and odd-numbered cell centers, which makes the code sensitive to saw-tooth-like error growth, thus needing an additional numerical dissipation term. The Runge–Kutta time-stepping scheme is applied to an extended version of the Euler equation:

$$\tilde{U}_{ijk}^{(n+1)} = \tilde{U}_{ijk}^{(n)} - (\Delta t/\Omega_{ijk})\{Q_{ijk}^{(n)} + D_{ijk}^{(n)}\} \quad (10)$$

where $Q_{ijk}^{(n)}$ denotes the flux balance of the cell as expressed by the integral terms of Eq. (9), and D_{ijk} introduces a small artificial viscosity for damping high-frequency oscillations.

When the solution of Eq. (10) for a steady state is concerned, then several acceleration techniques may be employed, which are extensively analyzed.[3]

III. Numerical Analysis of the Vortical Flowfields Around a Delta-Shaped Wing-Canard Configuration

The wing canard configuration used in this investigation is a cropped delta wing of 65-deg sweep angle coupled closely with a cropped delta canard of 60-deg sweep, both having a symmetrical cross-sectional profile with sharp leading edges as shown in Fig. 1. This model has already been studied in the international vortex flow experiment, thus having extensive experimental data that are illustrated in Refs. 28–30.

It is already mentioned in Sec. II.C that for delta-shaped configurations, O-O or C-O grid-topologies are very well-suited because of the natural grid clustering in the regions of high flow gradients. Due to the fact that the flowfield of a delta-shaped wing-canard combination is to be compared with that of a wing alone, the use of O-O or C-O grids would need separate detailed structuring for the wing alone and then with the canard placed ahead of the wing. However, with H-H grid-topology, properly layed around the wing and the canard, the same grid structure can be retained also for the canard-off case. This is simply realized by deleting the boundary condition $\boldsymbol{V} \cdot \boldsymbol{n} = 0$ on the canard surface, thus allowing the flow to go through the cells in this region. Thus, the use of H-H grids provided essential simplicity in the construction of the meshes and also uniformity in the handling of the wing with the canard off and on. In order to achieve higher precision in the flow resolution, especially in the regions of spi-

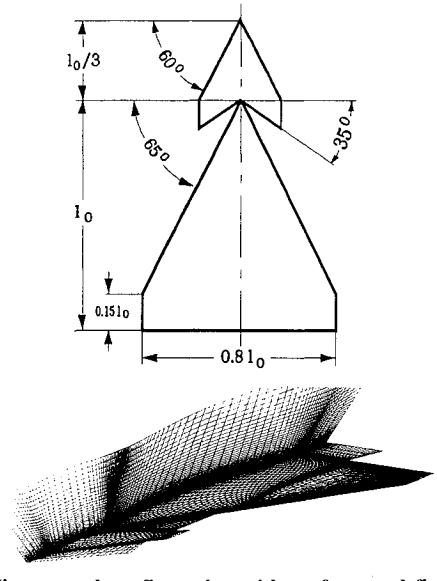

Fig. 1 Wing-canard configuration with surface- and field-grids for numerical study.

raling flows with high flow gradients, a large number of surface and field grids had to be provided for studying the details of the wing and canard vortices. Such grid refinement was carried out once for all.

The grid space around the wing was divided into two symmetrical blocks, one for the upper region and one for the lower region of the flowfield. Each block has 120 cells in the streamwise direction, 72 cells in half of the spanwise direction and 56 cells normal to the wing midsurface, thus amounting to a total of about 968,000 cells for the configuration having symmetrical onflow. The grid generation has been done by using transfinite interpolation followed by optimization procedure for orthogonality, based on the solution of the Poisson equations. The solution of the Euler equations in finite volume formulation was done by using the DLR-CEVCATS computer code, whereby several acceleration techniques[3] were employed. The CPU time for obtaining a complete field solution for symmetrical onflow at a given Mach number and incidence angle of the wing-canard combination amounted initially to 10 h on the Cray Y-MP, while by introducing multigrid techniques it could be reduced to about 2.5 h.

In order to determine the sensitivity of the computed solutions to different grid topologies and mesh fineness, extensive study has been made with the wing alone,[13,24] where different combinations of numerical schemes, grid topologies, and total number of cells were selected in turn. All the solutions for field quantities plotted spanwise or chordwise followed quite closely, thus lying in a very narrow band.

A. Structure of the Vortical Flowfields Around a Delta Wing with and Without Canard

Having the field solution around the wing-canard combination makes it easy to trace the canard and wing vortices spiraling downstream along with the flow, as shown in Fig. 2. For analyzing the vortical flow it is useful to have a plot of the flow quantities at a number of crosswise planes normal to the symmetric axis of the wing. The velocity fields V_C/V_∞ of the spiraling vortices at a cross-plane $\xi = 0.6$ are shown in Fig. 3 for $M_\infty = 0.85$ and $\alpha = 20$ deg, once for the wing alone and then for the wing-canard combination. Because both the wing and canard have sharp leading edges, it is evident that the Kutta condition at the edges are well-fulfilled by the spiraling flow. However, for round leading edges, an inviscid flow may not separate.[16,17] The isolines of c_p and $\Delta p_0/p_{0\infty}$ of the vortex fields are illustrated in Fig. 4.

It is evident that in the absence of the canard, the wing vortex is more intensive. This is due to the fact that the wing moving alone at a given incidence can impart more downward momentum to the medium than it can do with the closely coupled canard ahead of it. In case of a wing-canard combination, the canard first encounters the medium particles ahead of the wing; the imparted downward momentum causing canard lift yields the dipole effect or the strength of the bound vortices of the canard. As a consequence of the Canard downwash, the wing can now impart reduced downward momentum to the medium and produce somewhat less lift at a given angle of incidence, and hence, can emanate less intensive free vortices spiraling around the leading edges. Furthermore, the spiraling canard-vortex moving downstream over the wing induces downwash and upwash in inboard and outboard regions relative to its axis, and thus, further modifies the flowfield around the wing. Also, the mass-flux through the half-span of the wing gets involved into two vortices compared to one vortex for the wing-alone case, as is evident from Fig. 3. All these effects can be looked upon as the interaction of the vortex systems of the wing and canard.

The vortex system of the wing-canard configuration reveals that a part of the spiraling streamlines around the wing leading edge wraps around the canard-vortex, while for the wing-alone case they did join the wing vortex.

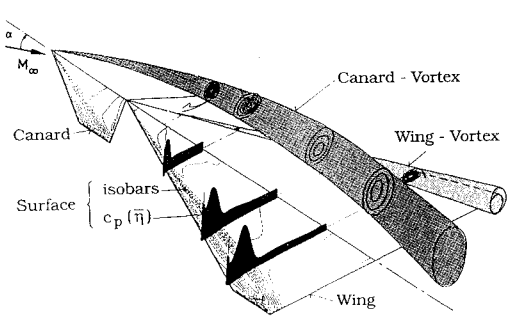

Fig. 2 Spiraling vortices and surface pressure distribution at M_∞ = 0.4 and α = 20 deg.

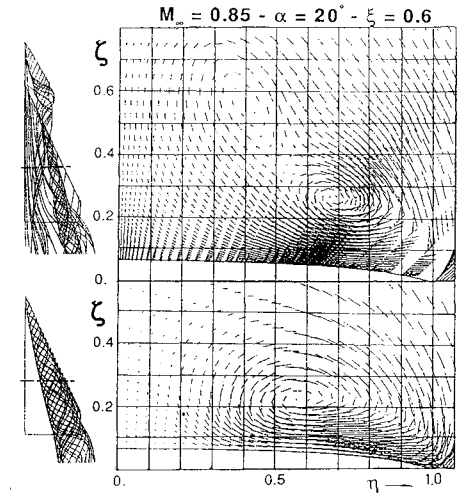

Fig. 3 Velocity field in the crossplane showing the spiraling vortices with the canard on and off.

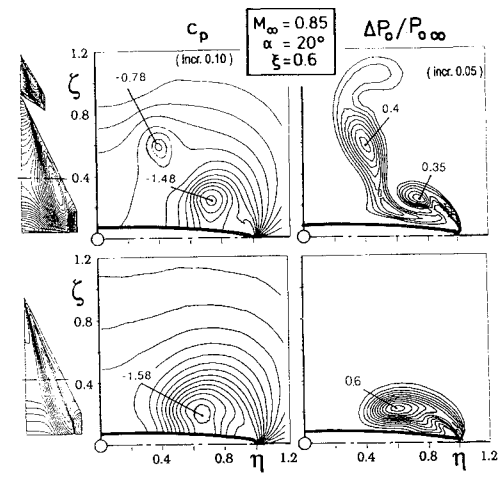

Fig. 4 Isolines of static and total pressure in a cross-plane with the canard on and off.

B. Analysis of the Flow and Pressure Gradients on the Upper Surface of the Delta Wing with and Without Canard

The formation of spiraling vortical flow over the moving delta wing at incidence contributes to highly curved surface streamlines of increased velocity. As a consequence the so-called bound vortices that are orthogonal to the streamlines take up curved shapes.[23] The increased surface velocity brings in an additional vortex lift. In case of a wing-canard combination, the vortical flow around the wing leading edge becomes less intensive, thus causing less negative c_p values on the wing upper surface as shown in Fig. 5. A comparison of

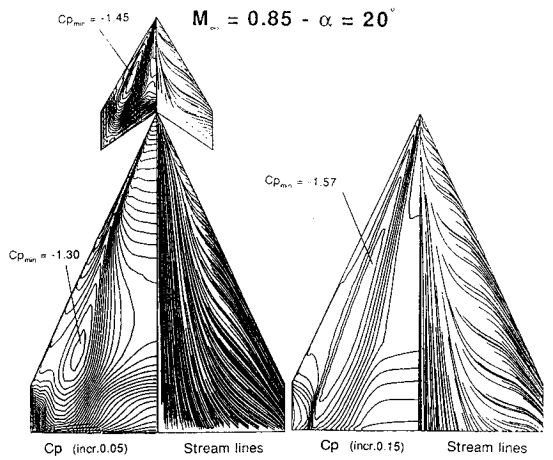

Fig. 5 Upper surface streamlines and isolines of static pressure with the canard on and off.

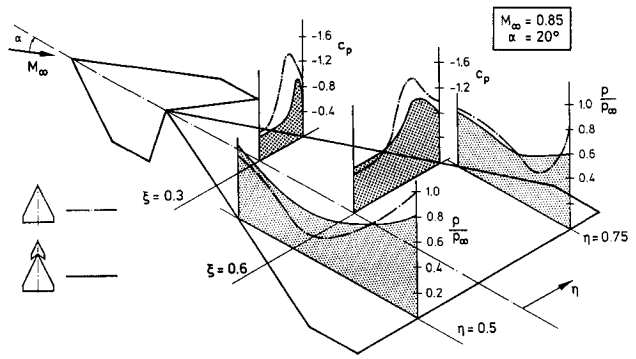

Fig. 6 Crosswise and chordwise upper surface pressure distributions with the canard on and off.

the streamlines and iso-c_p-lines of the wing upper surface for a canard-off and -on configuration confirm the findings of Sec. III.A. The induced upwash of the wing contributes to an accentuation of the dipole effect of the moving canard closely ahead of it, and the low surface pressure of the wing provides a favorable pressure field downstream of the canard trailing edge. The iso-c_p-lines and the streamlines of the canard upper surface as shown in Fig. 5 indicate that the canard produces substantial lift force, which can compensate the drop of the wing lift for a wing-canard combination.

In order to have a clear picture of the changes in pressure distributions on the upper surface of the wing for canard-on and -off configurations, a plot of the c_p values in a spanwise direction and of the p/p_∞ values in the chordwise directions are undertaken in Fig. 6. It is evident that the inducing effect of the canard-vortex system can be clearly recognized in the pressure distributions. The changes in the gradients towards the trailing edge can primarily be attributed to the diminished lift of the wing for canard-on configuration.

C. Validation of the Numerical Results on Pressure, Force, and Moment Coefficients by Comparison with Experimental Data

The field quantities yielded by the numerical solution of the Euler equations for flows around the wing-canard configuration have been extensively compared with the experimental results, both at subsonic and transonic onflows, thus confirming acceptable agreements of the crossflow velocity and pressure fields as well as of the losses in total-pressure in the spiraling vortices. The effect of viscosity on the surface flow is appreciable in the experimental data, and it will be purposeful to undertake a comparison of the pressure coefficients on the wing surface and the resulting forces and moments arising on the configuration as yielded by the numerical solutions and the measured values.

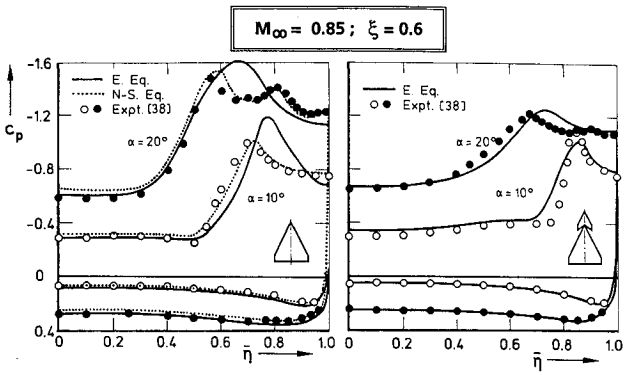

Fig. 7 Comparison of the crosswise surface pressure distribution as yielded by the numerical and experimental results.

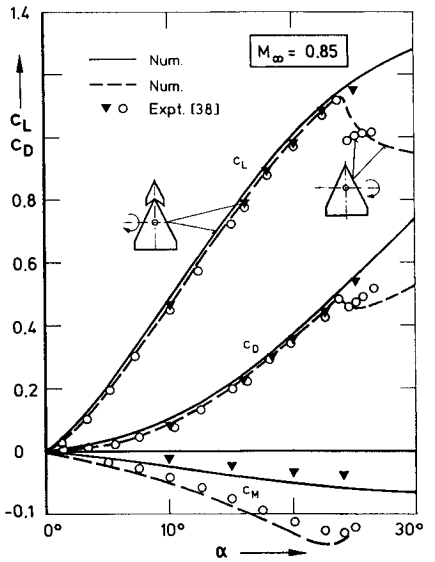

Fig. 8 Total forces and pitching-moment with the canard on and off. Comparison of numerical and experimental results.

The c_p distributions across a crossflow plane are shown in Fig. 7 for onflow Mach number M_∞ = 0.85 and angles of incidence α = 10 and 20 deg, both for the wing alone and the wing-canard configuration. While the solution of the Navier–Stokes equations[18] reproduces the experimental data very closely, it is evident that the solution of the Euler equations fails to capture the secondary vortex on the wing surface, arising due to the viscous effects. However, the c_p distribution yielded by the solution of the Euler equations takes up a typical run such that it partly overshoots and partly undershoots the curve yielded by the Navier–Stokes equations. As such, the resulting forces and moments on the wing surface are well-reproduced by the numerical solutions of the Euler equations, as has been demonstrated in Fig. 8. The $c_L(\alpha)$ curve clearly depicts that the additional vortex lift of the wing-canard configuration is maintained to quite large angles of incidence, thus giving it an outstanding aerodynamical property as compared to the wing-alone. The numerical results confirm the findings of the experimental data.

IV. Detailed Study of the Physical Relations in the Spiraling Vortical Flows Around a Delta-Shaped Wing-Canard Configuration

The field data as obtained from the solution of Euler equations and depicted in Sec. III allow detailed analysis of their interrelations. The dynamical and thermodynamical equations of compressible flow in an inviscid medium can be based on this.

The dynamical equations of motion have already been introduced in Eqs. (2) and (3). The field data $V = iv_r + jv_\vartheta + kv_x$ and p, ρ, T being known, the interrelations given in Eqs. (2–5) can be used for numerical analysis of the physical relations.

A. Accelerating Forces, Pressure Forces, and Vorticities for Establishing the Spiraling Flows over a Delta Wing

The numerical method based on Euler equations contains the momentum balance in the three coordinate directions x, y, z, or r, ϑ, x, as expressed in Eqs. (3) and (4). Hence, the field data in the crossflow planes, as depicted in Fig. 9, must confirm the balance of the radial accelerating forces in the $r - \vartheta$ plane, which is essential in establishing the spiraling flow. The radial components of the accelerating forces per unit mass are contained in the momentum equation:

$$\frac{\partial v_r}{\partial t} + v_r \frac{\partial v_r}{\partial r} + \frac{v_\vartheta}{r}\frac{\partial v_r}{\partial \vartheta} - \frac{v_\vartheta^2}{r} + \frac{\partial v_r}{\partial x} = -\frac{1}{\rho}\frac{\partial p}{\partial r} \tag{11}$$

Equation (11), having the dimension of m/s^2, may be rewritten in nondimensional form in the following version:

$$\frac{\partial v_r}{\partial \bar{\tau}} + \bar{v}_r \frac{\partial v_r}{\partial \bar{r}} + \frac{v_\vartheta}{\bar{r}}\frac{\partial v_r}{\partial \bar{r}} - \frac{v_\vartheta^2}{\bar{r}} + \frac{\partial v_r}{\partial \bar{x}} = -\frac{1}{\kappa M_\infty^2 \bar{\rho}}\frac{\partial \bar{p}}{\partial \bar{r}} \tag{12}$$

with $\bar{v} = v/V_\infty$, $\bar{\rho} = \rho/\rho_\infty$, $\bar{p} = p/p_\infty$, and $\tau = tv_\infty/r_0$, whereby the last term of the left-hand side (LHS) proves to be quite small compared to the others, and the first term is zero for a steady flowfield. Hence, the accelerating forces per unit mass may be expressed as

$$\bar{v}_r \frac{\partial \bar{v}_r}{\partial \bar{r}} + \frac{\bar{v}_\vartheta}{\bar{r}}\frac{\partial \bar{v}_r}{\partial \bar{r}} - \frac{\bar{v}_\vartheta^2}{\bar{r}} = \sum f_a = -\frac{1}{\kappa M_\infty^2 \bar{\rho}}\frac{\partial \bar{p}}{\partial \bar{r}} \tag{13}$$

Figure 10 elucidates clearly that the pressure force arising in the field just balances the required accelerating forces, which conforms to the numerical solution of the Euler equations. As comparison, the isentropic pressure force can be derived from the relation

$$-\bar{c}_p \frac{\partial T}{\partial r} = V\frac{\mathrm{d}V}{\mathrm{d}r} = -\frac{1}{\rho}\frac{\mathrm{d}p}{\mathrm{d}r}\bigg|_s \tag{14}$$

This can be rewritten in nondimensional form as

$$-\frac{\bar{c}_p}{\kappa R M_\infty^2}\frac{\partial \bar{T}}{\partial \bar{r}} = \bar{V}\frac{\partial \bar{V}}{\partial \bar{r}} = -\frac{1}{\kappa M_\infty^2 \bar{\rho}}\frac{\partial \bar{p}}{\partial \bar{r}}\bigg|_s \tag{15}$$

with $\bar{T} = T/T_\infty$ and $\bar{V} = V/V_\infty$.

It is evident from Fig. 10 that the isentropic pressure force is insufficient to establish a spiraling flow. The vortex flow being nonisentropic, the relations given by Eqs. (3) and (5) at once reveal the vorticity arising in the field. The missing magnitude of the accelerating force in the crossflow plane (r, ϑ) for ξ = const is contributed by the vorticity, which amounts to

$$\Delta f_a = \gamma_h \times v_h = -\left[\frac{1}{\rho}\frac{\mathrm{d}p}{\mathrm{d}r} - \bar{c}_p \frac{\mathrm{d}T}{\mathrm{d}r}\right] \tag{16}$$

Writing in nondimensional form

$$\Delta \bar{f}_a = \bar{\gamma}_h \times \bar{v}_h = -\frac{1}{\kappa M_\infty^2}\left[\frac{1}{\rho}\frac{\partial \bar{p}}{\partial \bar{r}} - \frac{\bar{c}_p}{R}\frac{\partial \bar{T}}{\partial \bar{r}}\right] \tag{17}$$

where $\Delta \bar{f}_a = \Delta f_a r_0/V_\infty^2$, $\bar{\gamma}_h = \gamma_h r_0/V_\infty$, and $\bar{v}_h = v_h/V_\infty$. From Fig. 10 it is evident that the vorticity in the wing vortex

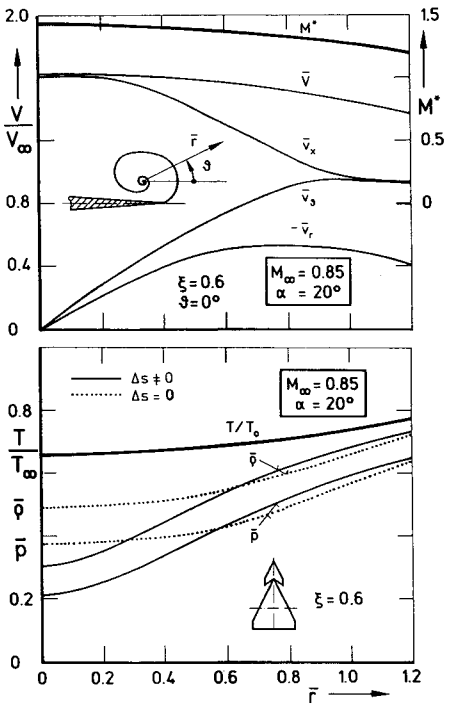

Fig. 9 Velocity components and state variables in a cross-plane of the wing-canard configuration.

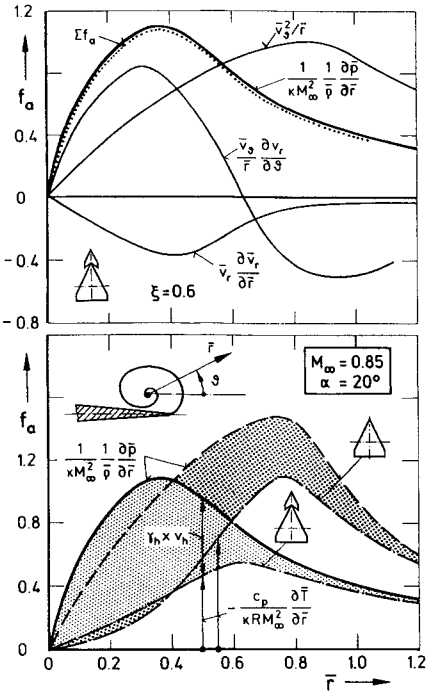

Fig. 10 Accelerating forces in the spiraling flow depicting the required pressure forces and vorticities for setting in the spiraling.

is significantly influenced by the presence of the canard vortex, needing less Δf_a to establish the spiraling as compared to the case of the wing alone.

Although the numerical analysis confirms clearly the nature of momentum balance in the spiraling vortical flow arising over a delta wing, further convincing details can be obtained by looking into the essential physics of the flow from the viewpoint of causality and effect.

When spiraling flows arise in an unbounded inviscid medium under the superimposition of a two-dimensional sink on a potential vortex flow, the resulting velocity and pressure

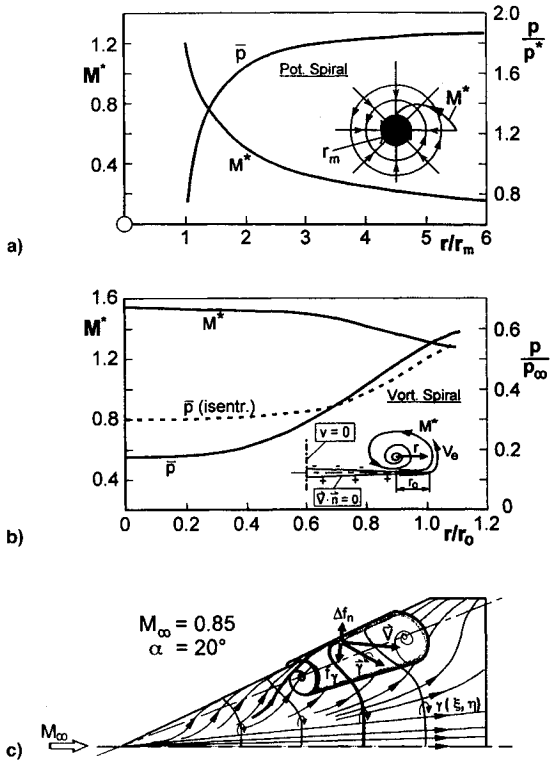

Fig. 11 Natural spiraling flow in an unbounded medium and the vortical flow of a delta wing under severe constraints.

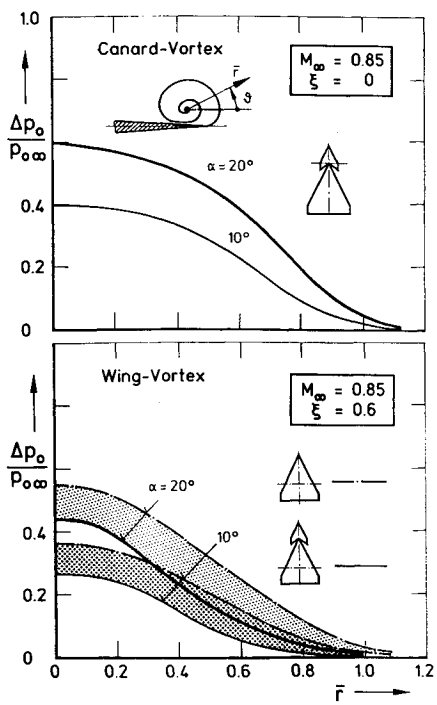

Fig. 12 Loss of total pressure in the spiraling flows arising at the canard and the wing with the canard on and off.

distributions in the field are depicted in Fig. 11a. It is evident that the required accelerating force in the radial direction is fully contributed by the pressure gradient.

In case of the spiraling flow setting in around a delta wing, it is subjected to three severe constraints: 1) the high fluid velocity at the edge caused by the dipole effect of the lifting surface, 2) the kinematic condition $\boldsymbol{V}\cdot\boldsymbol{n} = 0$ at the wing surface close to the vortex, and 3) the condition $v = 0$ at the

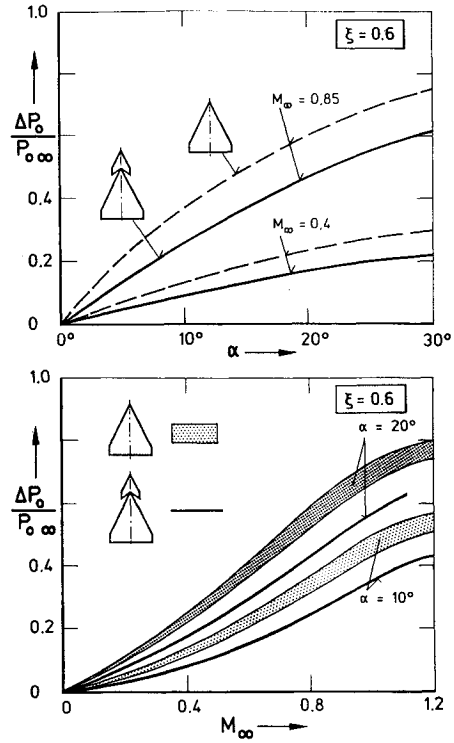

Fig. 13 Loss of total pressure at the vortex core as a function of α and M_∞ with the canard on and off.

vertical symmetry plane of the wing. Accordingly, the velocity and pressure distributions that arise over a radial direction take the shapes as shown in Fig. 11b. The indicated isentropic pressure distribution in the field (dotted line) can in no way supply the full accelerating force needed for spiraling, as is elucidated in Ref. 14.

Due to the dipole effects imposed by a moving lifting surface, bound vortices arise on it in a spanwise direction, and they become highly curved in case of a delta wing at high incidence. According to Kelvin's vortex law these vortex lines continue as free vortices in the spiraling flow as illustrated in Fig. 11c. It is by no means compelling that the vorticity vectors should align with the velocity vectors of the spiraling streamlines. An alignment is usual only in a force-free wake, e.g., in the downstream of the trailing edge of a large span wing. The resolution of the force vectors in the spiraling flow depicts clearly that the vortex force f_γ act in the right direction to compensate for the missing accelerating force Δf_a, as described by Eq. (17). The required disalignments between $\boldsymbol{\gamma}$ and $\boldsymbol{V}$ vectors are called in according to the natural process in the flowfield, as confirmed by the numerical analysis.

B. Loss of Total Pressure in the Spiraling Vortices of a Delta Wing with and Without Canard

From numerical solutions of the field equations, as well as from the experimental test, it is confirmed that the radial accelerating force for the spiraling of the vortical flows around a delta-shaped wing is partly supported by the vorticity force, which give rise to entropy changes as defined by Eq. (5).

Using the second law of thermodynamics, one can derive the following relation for the entropy change, and therefrom the loss in total pressure:

$$\frac{\Delta s}{R} = \frac{\kappa}{\kappa - 1} /\!\!/ \frac{T}{T_\infty} - /\!\!/ \frac{p}{p_\infty} \tag{18}$$

This yields

$$e^{-\Delta s/R} = \frac{p/p_\infty}{(T/T_\infty)^{\kappa/(\kappa-1)}} \tag{19}$$

The loss of total pressure in an adiabatic flowfield is given by the relation

$$\frac{\Delta p_0}{p_{0\infty}} = 1 - \frac{p_0}{p_{0\infty}} = 1 - e^{-\Delta s/R} \tag{20}$$

The loss of total pressure in the spiraling flows of the delta wing with and without canard is depicted in Figs. 12 and 13 for various onflow conditions, revealing clearly that the canard has a favorable effect on the wing flow such that the wing vortex keeps up more total pressure on its way downstream, and is thus less amenable to breakdown. For the wing alone, a plot of the total pressure losses for various combinations of numerical schemes and grid topologies, tested earlier, has been undertaken, thus yielding a narrow band, of which the mean line can be used for comparison with the results obtained for the wing-canard combination.

C. Flow Gradients Along the Vortex Axis Initiating Saddle Points with Flow Reversal and Vortex Bursting

The onflow condition along the vortex core may be studied by applying the following basic equations:

$$v_r \frac{\partial v_x}{\partial r} + \frac{v_\vartheta}{r}\frac{\partial v_x}{\partial \vartheta} + v_x \frac{\partial v_x}{\partial x} = -\frac{1}{\rho}\frac{\partial p}{\partial x}$$
$$T\frac{ds}{dx} = \gamma_c \times v_c = -\frac{1}{\rho}\frac{dp}{dx} + \bar{c}_p \frac{dT}{dx} \tag{21}$$

with $\gamma_c = \gamma_r + \gamma_\vartheta$ and $v_c = v_r + v_\vartheta$.

Furthermore, the temperature distribution T/T_0 along the vortex core can be determined from the velocity distribution by using the simple relation for adiabatic flow:

$$(T/T_0) + [(\kappa - 1)/(\kappa + 1)]M^{*2} = 1 \tag{22}$$

The pressure and velocity distribution along the axis of the wing vortex for the canard-off case is shown in Fig. 14 once more, for comparison with the canard-on configuration. The inherent adverse pressure gradient and flow deceleration in regions near the wing trailing edge is a typical feature of slender delta wings, as depicted in Fig. 5. The total pressure p_0 in the vortex core being subjected to severe loss, especially at large incidence and high onflow Mach number of the wing, the fluid particles lose all their kinetic energy in overcoming the steep pressure gradient and cause the formation of the first saddle point on the vortex axis, close downstream of the trailing edge. The flowfield is three dimensional, and so the saddle point is axisymmetric in the region close to the vortex axis. The existing pressure gradient upstream of the saddle point gives rise to a reverse flow and accelerates it, thus encountering the oncoming flow from upstream. Hence, a second saddle point of similar nature with the streamlines directed radially outwards in the cross-plane comes into being. When the reverse flow is moderate it may cause only a bulging of the vortex core, while with strong reverse flow the radial streamlines of the upstream saddle point cause a total breakdown of the vortex. These findings are also discussed[14] and compared with the physical phenomena occurring in electromagnetic fields and are also well-validated by the experimental results.[35,36] With increasing angle of incidence both saddle points move upstream along the vortex axis.

For steady motion of the wing, the vortical flowfield does possess a steady character. When vortex breakdown occurs, the unsteady nature of the flow remains more or less confined to the burst region. The governing equations and computational algorithm used for this investigation were formulated to achieve steady-state solutions. In the region of vortex breakdown the flowfield induced by the vortex becomes unsteady and the computed flow variables exhibit on oscillatory motion of periodic character. Hence, the solution converges to results that are globally stationary, but locally unsteady, and hence, converged solutions are assumed once the computed flow variables reach corresponding steady state in terms of their mean values. Extensive numerical–experimental correlation studies were carried out[27] in order to validate this

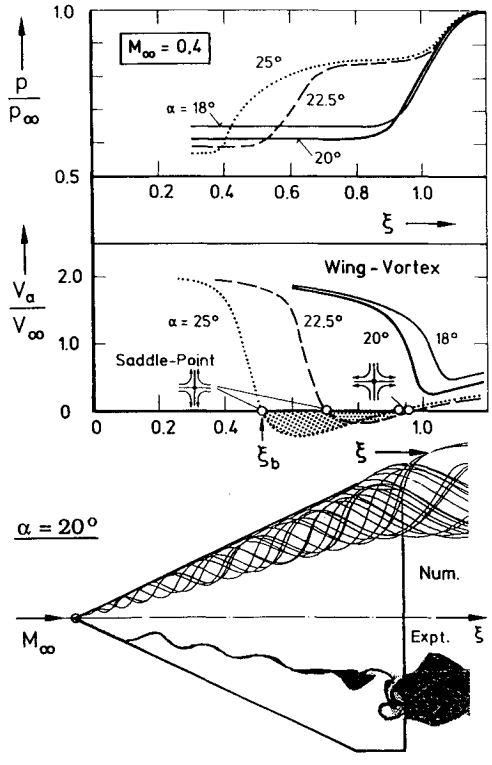

Fig. 14 Numerical analysis of the condition of vortex breakdown, confirming flow reversal with saddle points.

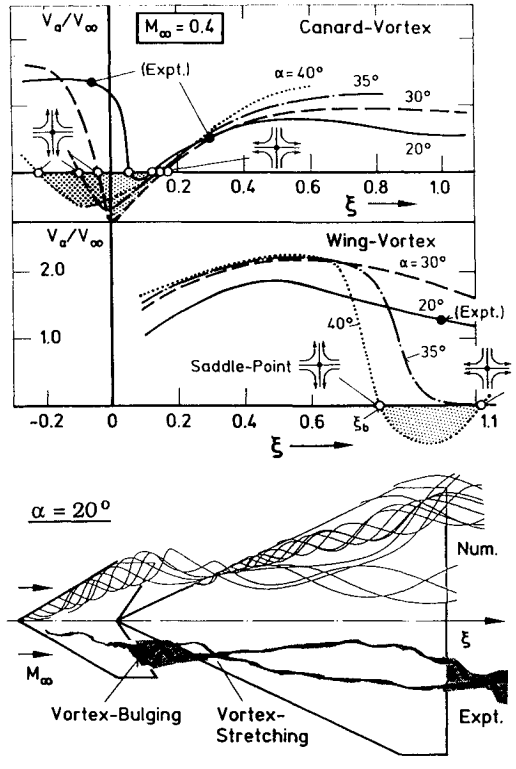

Fig. 15 Numerical analysis of the favorable effect of the canard in delaying wing-vortex breakdown.

procedure for the computation of vortical flows up to vortex breakdown.

In case of a wing-canard configuration the canard vortex is formed under a similar condition as for a delta wing alone, however, with some favorable effect of the wing pressure field decreasing the adverse pressure gradient at the canard trailing edge region and also accelerating the flow of the canard vortex core over the wing, as can be seen from Fig. 15. Again, the run of the numerical curves are well-confirmed by experimental data.[36]

For studying the flow conditions around the wing of the wing-canard combination at high angles of incidence, it is essential to look into the behavior of the vortex flow, especially in the region of the wing rear part, as has been elucidated in Fig. 15. Due to less loss in total pressure and less adverse pressure gradients encountered by the vortex flow, as has been analyzed in previous sections and depicted in Fig. 13 and Fig. 6, the axial velocity in the vortex core remains upright until $\alpha \geq 30$ deg, only beyond $\alpha = 35$ deg does the strong deceleration set in, causing the appearance of saddle points with flow reversal and vortex bursting, when $\alpha \geq 40$ deg. Less adverse pressure gradient in the wing rear region causes less separation of a viscous flow on the wing upper surface. These are analyzed[27] and are the main findings explaining the aerodynamic superiority of a wing-canard combination compared to the wing alone.

It is obvious that the beneficial effect of the canard vortex on the wing flow continues, even long after the first appearance of vortex bulging over the canard at $\alpha = 20$ deg, as illustrated in Fig. 15, it being subjected to subsequent stretching effects over the wing due to the favorable low pressure. For angle of incidence $\alpha > 30$ deg, the canard vortex undergoes stronger bulging and then a breakdown.

At high angles of incidence the canard vortex can be stabilized by setting the canard with a negative angle so that flow reversal in the canard vortex is highly suppressed until $\alpha \geq 40$ deg, as shown in Fig. 16. However, it is evident that the axis of the canard vortex over the wing is now shifted upward, and hence, the negative setting of the canard remains

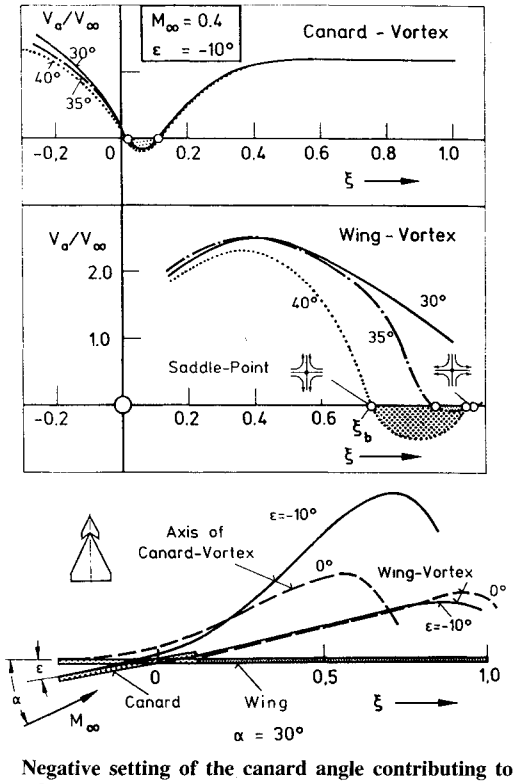

Fig. 16 Negative setting of the canard angle contributing to a stabilization of the vortex system of the wing.

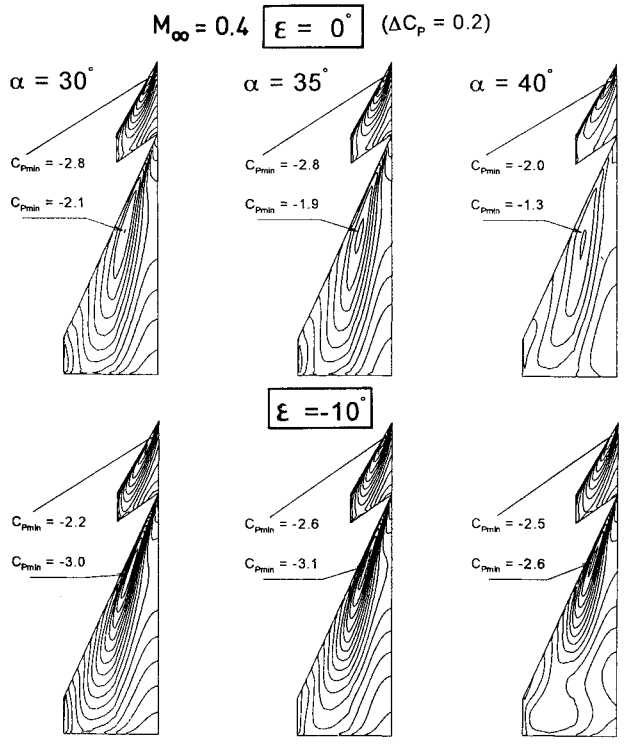

Fig. 17 Isolines of upper surface static pressure confirming the beneficial effect of the negative setting of the canard on the wing flow.

ineffective for the flow at the rear part of the wing, when $\alpha \geq 30$ deg. The corresponding pressure distribution on the upper surface of the wing-canard configuration at moderate and high angles of incidence are depicted in Fig. 17 for the canard setting with $\varepsilon = 0$ and -10 deg.

The numerical study and analysis confirms all the findings of the wind-tunnel experiments and also of flight tests, concerning the outstanding aerodynamic properties of delta-shaped wing-canard configurations.

V. Conclusions

In order to study the complete details of a flowfield it is essential to consider the effects of viscosity, especially in regions of high cross gradients in turbulent flows. However, the amount of effort to solve the Navier–Stokes equations for complex flowfields may sometimes be too high. When the effects of viscosity and heat conductivity remain confined to small regions, the solution of the Euler equations proves to be quite useful in yielding the main features of a flowfield, especially when slender delta wings are concerned. Having this objective in view, numerical studies on the flowfields of delta wings and delta-shaped wing-canard configurations have been pursued intensively in recent years.

In this article, special emphasis has been put on analyzing the basic physics of the vortical flows, concerning the accelerating forces and the loss of total pressure needed for setting in the spiraling motion. Further characteristic features are the interactions of the vortex system and the condition that leads to an essential stabilization of the wing vortex against its breakdown until at much higher incidence angles. The field data yielded by the solution of the Euler equations are adequate to establish dynamical and thermodynamical relations in the spiraling flows, which elucidate all the findings known until now from experiments, including the condition of flow deceleration and reversal along the vortex axis preceding the bulging and breakdown of the vortex structure. For analyzing the details of the complex flows in the region containing reverse flow with vortex bursting, it is essential to use numerical codes for unsteady flows with proper simulation of the time

steps. Also, when the numerical methods for solving the field equations can be extended to include efficient and reliable automatic grid adaptive techniques, test cases may be taken up by using the solution of Navier–Stokes equations and comparing them with the present results.

References

[1]Lax, P. D., and Wendroff, B., "System of Conservation Laws," *Communications on Pure and Applied Mathematics*, Vol. 13, No. 2, 1960, pp. 217–237.

[2]Jameson, A., Schmidt, W., and Turkel, A., "Numerical Solution of the Euler Equations by Finite Volume Method Using Runge-Kutta Time Stepping Schemes," AIAA Paper 81-1259, June 1981.

[3]Rossow, C.-C., "Berechnung von Strömungsfeldern durch Lösung der Euler Gleichungen mit einer erweiterten Finite-volumen Diskretisierungsmethode," DLR-FB 89-38, July 1989.

[4]MacCormack, R., "A Numerical Method for Solving the Equations of Compressible Viscous Flow," *AIAA Journal*, Vol. 20, No. 9, 1982, pp. 1275–1281.

[5]MacCormack, R., "Current Status of Numerical Solutions of the Navier-Stokes Equations," AIAA Paper 85-0032, Jan. 1985.

[6]Radespiel, R., Rossow, C.-C., and Swanson, R. C., "An Efficient Cell-Vertex Multigrid Scheme for the Three-Dimensional Navier-Stokes Equations," *AIAA Journal*, Vol. 28, No. 8, 1990, pp. 1464–1472; also NASA-TM 101558, 1989.

[7]Thompson, J. F., Warsi, Z. U. H., and Mastin, C. W., *Numerical Grid Generation. Foundation and Applications*, North-Holland, New York, 1985.

[8]Eriksson, L. E., "Generation of Boundary-Conforming Grids Around Wing-Body Configurations Using Transfinite Interpolation," *AIAA Journal*, Vol. 20, No. 10, 1982, pp. 1313–1320.

[9]Sonar, Th., and Radespiel, R., "Geometric Modelling of Complex Aerodynamic Surfaces and Three-Dimensional Grid Generation," *Proceedings of the 2nd International Conference on Numerical Grid Generation*, Pineridge, Swansea, Wales, UK, 1988.

[10]Murman, E. M., and Rizzi, A., "Application of Euler Equations to Sharp Edge Delta Wings with Leading Edge Vortices," *AGARD Fluid Dynamics Panel Symposium on Applications of Computational Fluid Dynamics in Aeronautics*, 1986, pp. 15.1–15.13 (AGARD CP-412).

[11]Powell, K., Murman, E., Perez, E., and Baron, J., "Total Pressure Loss in Vortical Solutions of the Conical Euler Equations," AIAA Paper 85-1701, July 1985.

[12]Kumar, A., and Das, A., "Computation of Vortex Flow on a Delta-Wing at Transonic Speed," *IUTAM Symposium Transonicum III*, 1988, pp. 317–328.

[13]Longo, J. M. A., "The Role of the Numerical Dissipation on the Computational Euler Equations Solutions for Vortical Flows," AIAA Paper 89-2232, July 1989.

[14]Das, A., "Analysis of Spiraling Vortical Flows Around Slender Delta Wings Moving in an Inviscid Medium," *ZAMM*, Vol. 71, No. 11, 1991, pp. 465–471.

[15]Rizetta, D. P., and Shang, J. S., "Numerical Simulation of Leading Edge Vortex Flows," *AIAA Journal*, Vol. 24, No. 2, 1986, pp. 237–245.

[16]Newsome, R. W., and Kandil, O. A., "Vortical Flow Aerodynamics—Physical Aspects and Numerical Simulation," AIAA Paper 87-2205, Jan. 1987.

[17]Kandil, O. A., Chuang, A. H., and Shifflette, J. M., "Finite Volume Euler and Navier-Stokes Solvers for Three-Dimensional and Conical Vortex Flows over Delta Wings," AIAA Paper 87-0041, Jan. 1987.

[18]Longo, J. M. A., "Simulation of Complex Inviscid and Viscous Vortex Flow," *IUTAM Symposium on Fluid Dynamics of High Angle of Attack*, Springer–Verlag, Berlin, 1992, pp. 363–373.

[19]Agrawal, S., Barnett, R. M., and Robinson, B. A., "Investigation of Vortex Breakdown on a Delta Wing Using Euler and Navier-Stokes Equations," *AGARD Fluid Dynamics Panel Symposium on Vortex Flow Aerodynamics*, 1990, pp. 24.1–24.12 (AGARD-CP-494).

[20]Das, A., and Longo, J. M. A., "Numerical Computation of Vortical Flow Fields of Double-Delta Wings Moving in a Compressible Medium," *ZAMM*, Vol. 74, No. 10, 1994, pp. 475–486.

[21]Krause, E., and Liu, C. H., "Numerical Studies of Incompressible Flow Around Delta and Double-Delta Wings," *Zeitschrift für Flugwissenschaften und Weltraumforschung*, Vol. 13, Nos. 9/10, 1989, pp. 291–301.

[22]Eriksson, L., and Rizzi, A., "Computation of Vortex Flow Around a Canard-Delta Wing Combination," *Proceedings of the 5th GAMM Conference on Numerical Methods in Fluid Mechanics*, Braunschweig, Germany, 1983, pp. 65–80.

[23]Scherr, S., and Das, A., "Basic Analysis of the Flow Fields of Slender Wings Using the Euler Equations," *Proceedings of the 16th Congress of the International Council of the Aeronautical Sciences*, Vol. 2, 1988, pp. 1428–1436.

[24]Longo, J. M. A., and Das, A., "Numerical Simulation of Vortical Flows over Close-Coupled Canard-Wing Configuration," AIAA Paper 90-3003, Aug. 1990.

[25]Longo, J. M. A., and Das, A., "Numerical Study of a Delta Wing in Sideslip," Arbeitsgemeinschaft STAB Jahresbericht 1992, pp. 101, 102.

[26]Hilgenstock, A., and Vollmers, H., "On the Simulation of Compressible Turbulent Flows past Delta Wings, Delta Wing-Body and Delta-Wing Canard," *AGARD FDP Symposium on Vortex Flow Aerodynamics*, 1990, pp. 7.1–7.14 (AGARD-CP-494).

[27]Longo, J. M. A., "Untersuchungen der Umströmung von Deltaflügelkonfigurationen mit und ohne Canard durch numerische Lösung der Euler-Gleichungen," *Zentrum für Luft- und Raumfahrttechnik, Forschungsbericht 93-09*, Technische Universität, Braunschweig, Germany, 1993.

[28]Hummel, D., "Documentation of Separated Flows for Computational Fluid Dynamics Validation," *AGARD Fluid Dynamics Panel Symposium on Validation of Computational Fluid Dynamics*, Vol. 2, 1988, pp. 15.1–15.24 (AGARD-CP-437).

[29]Elsenaar, A., Hjelmberg, L., Bütefish, K., and Bannink, W. J., "The International Vortex Flow Experiment," *AGARD Fluid Dynamics Panel Symposium on Validation of Computational Fluid Dynamics*, Vol. 1, 1988, pp. 9.1–9.23 (AGARD-CP-437).

[30]Drougge, G., "The International Vortex Flow Experiment for Computer Code Validation," *Proceedings of the 16th Congress of the International Council of the Aeronautical Sciences*, Vol. 1, 1988, pp. 35–46.

[31]Brennenstuhl, U., and Hummel, D., "Vortex Formation over Double-Delta Wings," *Proceedings of the 13th Congress of the International Council of the Aeronautical Sciences*, Vol. 2, 1982, pp. 1133–1146.

[32]Radespiel, R., and Quast, A., "Kraftmessungen, Druckverteilungen und Strömungssichbarmachung am Raumgleitermodell FALKE im Niedergeschwindigkeitsbereich," DLR IB-129-89/37, 1989.

[33]Bornemann, W. E., and Surber, T. E., "Aerodynamic Design of the Space Shuttle Orbiter," *AGARD Fluid Dynamics Panel Symposium on High Angle of Attack Aerodynamics*, 1978, pp. 11.1–11.24 (AGARD-CP-247).

[34]Esch, H., "Force Measurements on Four 1:100 HERMES Shape-Derivatives at Subsonic and Supersonic Mach Numbers," DLR-IB 39113-89-C-21, 1989.

[35]Elsenaar, A., and Hoijemakers, H. W. M., "An Experimental Study of the Flow over a Sharp Edged Delta Wing at Subsonic and Transonic Speeds," *AGARD FDP Symposium on Vortex Flow Aerodynamics*, 1990, pp. 15.1–15.19 (AGARD-CP-494).

[36]Oelker, H.-Chr., "Aerodynamische Untersuchungen an kurzgekoppelten Entenkonfigurationen bei symmetrischer Anströmung," *Zentrum für Luft- und Raumfahrttechnik, Forschungsbericht 90-01*, Technische Universität, Braunschweig, Germany, 1990.

[37]Lamb, H., *Hydrodynamics*, 6th ed., Cambridge Univ. Press, Cambridge, England, UK, 1957.

[38]Liepmann, H., and Roshko, A., *Elements of Gasdynamics*, Wiley, New York, 1957.

[39]Prandtl, L., and Tietjens, O., *Fundamentals of Hydro & Aerodynamics*, Dover, New York, 1934.

[40]Schlichting, H., *Boundary-Layer Theory*, 6th ed., McGraw–Hill, New York, 1968.

[41]Durand, W. F., *Aerodynamic Theory*, Vols. II and III, Dover, New York, 1963.

[42]Ames, W. F., *Numerical Methods for Partial Differential Equations*, Academic, New York, 1977.